Mon. Not. R. Astron. Soc. **000**, 000–000 (2008) Printed 4 January 2012 (MN LaTeX style file v2.2)

arXiv:1201.0369v1 [astro-ph.HE] 1 Jan 2012

Measures of cosmic-ray energy densities in galaxies

Massimo Persic[1,2], Yoel Rephaeli[3,4]
[1] *INAF/Osservatorio Astronomico di Trieste, via G.B.Tiepolo 11, I-34143 Trieste, Italy*
[2] *INFN Sezione di Trieste, Trieste, Italy*
[3] *School of Physics & Astronomy, Tel Aviv University, Tel Aviv 69978, Israel*
[4] *Center for Astrophysics and Space Sciences, University of California at San Diego, La Jolla, CA 92093, USA*

Accepted ... ... Received ... ... ; in original form ... ...

ABSTRACT

The energy density of cosmic ray protons (CRp) in star-forming galaxies can be estimated from *(i)* π^0-decay γ-ray emission, *(ii)* synchrotron radio emission, and *(iii)* supernova rates. For most of the galaxies for which values of all these quantities are known, the three methods yield consistent energy density estimates, ranging from $\mathcal{O}(10^{-1})\,\mathrm{eV\,cm^{-3}}$ in galaxies with low star-formation rates, to $\mathcal{O}(10^{2})\,\mathrm{eV\,cm^{-3}}$ in galaxies with high star-formation rates. The only cases for which the methods do not agree are the composite starburst/Seyfert 2 galaxy NGC1068, whose γ-ray emission originates in black-hole accretion rather than star formation, and the Small Magellanic Cloud, where the discrepancy between measured and estimated CRp energy density may be due to a small CR confinement volume.

Key words: Galaxies: cosmic rays – Galaxies: gamma-ray – Galaxies: spiral – Galaxies: star formation

1 INTRODUCTION

Active star formation in galaxies leads to production of cosmic ray protons and electrons (CRp, CRe) via the Fermi-I diffusive shock acceleration mechanism in supernova (SN) remnants (Fermi 1954; Ginzburg & Syrovatskii 1964; Bell 1978; Protheroe & Clay 2004).

Timescales of starburst (SB) activity in galaxies are comparable to galactic dynamical timescales, $\tau_{\rm SB} \sim \tau_{\rm dyn} \sim 10^8$ yr. On the other hand, in a SB region the characteristic timescales for protons to gain energy (by the Fermi-I acceleration process), and to lose it by collisions with thermally-distributed protons (leading to pion production and decay) and advection, are $\tau_+ \sim \tau_- \sim 10^5$ yr. Indeed, assuming the Fermi-I process to be at work in a SN remnant, $\tau_+ \equiv E/\dot{E} = (\Delta E/E)^{-1}\Delta t = \beta^{-1}\Delta t = (10/\beta_{0.1})\,\Delta t \sim 10^5$ yr, where $\Delta t \sim 10^4$ yr is a typical SN remnant lifetime, and $\beta_{0.1}$ is the speed of the SN ejecta in units of $0.1\,c$. The main energy-loss timescale is largely determined by the SN-driven outflow emanating from the SB region, i.e. $\tau_- \sim \tau_{\rm out} \sim 10^5$ yr; thus, $\tau_+ \sim \tau_- << \tau_{\rm SB}$.

The respective lengths of these timescales suggest that in galaxies, during typical episodes of star formation, a balance can be achieved by CR between energy gains and losses. Under basic hydrostatic and virial equilibrium conditions in a galaxy, a minimum-energy configuration of magnetic field and CR may be attained; this is equivalent to having CR and magnetic fields in (approximate) energy equipartition (e.g., Longair 1994 – but see Beck & Krause 2005 for a critical view).

The equipartition assumption enables deduction of the CRp energy density in star forming galaxies, $U_{\rm p}$ (the main contribution to the particle energy density), indirectly from the electron energy density (from radio synchrotron measurements) if a theoretically motivated injection proton-to-elecron (p/e) ratio is assumed.

Another way to derive $U_{\rm p}$ is based on measuring the GeV-TeV γ-ray emission, which is largely from CRp interactions with ambient gas protons, which produce neutral (π^0) and charged pions; π^0 decays into γ-rays. So γ-ray measurements provide a direct measurement of $U_{\rm p}$. Only recently have such measurements been possible for star-forming galaxies – and only for a handful of sources (see below).

Third, since energy-loss timescales are shorter than star-formation timescales, $U_{\rm p}$ can be estimated from the observed rate of core-collapse SN and the deduced residency time of CRp in the insterstellar medium – once a fraction of SN kinetic energy that is channeled into particle acceleration has been assumed.

This paper describes measures of galactic CR energy densities based on the methods outlined above. Although not strictly independent, these methods are based on very different observables to estimate $U_{\rm p}$: radio emission, HE γ-ray emission, and the rate of core-collapse SN. We find that the three methods yield consistent results on $U_{\rm p}$ for a sample of 10 galaxies with widely varying levels of star formation activity from quiescent to intense starbursts. These are the only galaxies for which γ-ray data (plus radio data and SN rates) are available (see Table 1). After reviewing the radio, γ-ray, and SN methods (sect. 2,3,4), the corresponding values of $U_{\rm p}$ are presented in section 5. The results are discussed in section 6 and summarized in section 7.

2 PARTICLES AND MAGNETIC FIELDS

CRe populations consist of primary (directly accelerated) and secondary (produced via $\pi^{\pm}$ decays) electrons. While the exact form of the steady-state CRe energy spectrum is not a single power law, at high energies the flattening of the spectrum due to Coulomb losses can be ignored, justifying the use of the approximate single power-law form. Let then the combined (primary plus secondary) CRe spectral density distribution be a single power-law

$$N_{\rm e}(\gamma) \;=\; N_{e,0}\,(1+\chi)\;\gamma^{-q}\,, \tag{1}$$

where the electron Lorentz factor γ is in the range $\gamma_1 \leq \gamma \leq \gamma_2$, $N_{e,0}$ is a normalization factor of the primary electrons, χ is the secondary-to-primary electron ratio, and $q \geq 2$ is the spectral index (the equality holds in the strong-shock limit of the Fermi-I acceleration process).

Ignoring the contribution of low-energy electrons with $\gamma < \gamma_1$, the electron energy density is $U_{\rm e} = N_{e,0}\,(1+\chi)\,m_{\rm e}c^2 \int_{\gamma_1}^{\gamma_2} \gamma^{1-q}{\rm d}\gamma$, where γ_2 is an upper cutoff whose exact value is irrelevant in the the limit of interest $\gamma_2 >> \gamma_1$. For $q > 2$ and $\gamma_2 >> \gamma_1$,

$$U_{\rm e} \simeq N_{e,0}(1+\chi)m_{\rm e}c^2\gamma_1^{2-q}/(q-2)\,. \tag{2}$$

For a population of electrons described by Eq.(1), traversing a homogeneous magnetic field of strength B in a region with (a spherically equivalent) radius $r_{\rm s}$ located at a distance d, and emitting a 1 GHz synchrotron radiation flux of $f_{1\,{\rm GHz}}$ Jy, standard theory yields

$$N_{\rm e,0}(1+\chi) \;=\; 5.72\times10^{-15}\;\psi\;a(q)^{-1}\;B^{-\frac{q+1}{2}}\;250^{\frac{q-1}{2}} \tag{3}$$

where $a(q)$ is defined and tabulated in, e.g., Tucker (1975) and ψ is defined as $\psi \equiv (\frac{r_{\rm s}}{0.1\,{\rm kpc}})^{-3}(\frac{d}{\rm Mpc})^{2}(\frac{f_{1\,{\rm GHz}}}{\rm Jy})$. From Eqs.(2, 3) we then derive

$$U_{\rm e} \;\simeq\; \frac{2.96}{(1+\chi)}\times10^{-22}\,250^{\frac{q}{2}}\,\psi\,\frac{\gamma_1^{-q+2}}{(q-2)\;a(q)}\;B^{-\frac{q+1}{2}}\,. \tag{4}$$

In order to compute $U_{\rm e}$ from Eq.(4) we need to specify γ_1 and B. To do so we make the following assumptions:
(i) We assume that the low-energy limit of the electron power-law spectrum, γ_1, marks the transition (for decreasing energy) from Coulomb ((Gould 1972; Rephaeli 1979) to synchrotron losses. For an electron of energy γ, the synchrotron loss rate is

$$-\Big(\frac{{\rm d}\gamma}{{\rm d}t}\Big)_{\rm syn} \;=\; 1.30\times10^{-21}\gamma^2\left(\frac{B}{\mu G}\right)^2\,{\rm s}^{-1} \tag{5}$$

whereas the Coulomb loss rate is

$$-\Big(\frac{{\rm d}\gamma}{{\rm d}t}\Big)_{\rm coul} \;=\; 1.2\times10^{-12}n_{\rm e,th}\left[1.0+\frac{\ln{(\gamma/n_{\rm e,th})}}{75}\right]{\rm s}^{-1}\,. \tag{6}$$

(Rephaeli 1979; Sarazin 1999). We then simply assume that CRe lose energy via Coulomb scattering for $\gamma < \gamma_1$ and via synchrotron cooling for $\gamma > \gamma_1$.
(ii) We assume equipartition between the energy densities of particles (CR electrons and protons) and magnetic fields, $U_{\rm p} + U_{\rm e} \;=\; B^2/8\pi$. This condition may actually be attained by strong coupling between all the relevant degrees of freedom in the SB region. In terms of the CR p/e energy density ratio, κ, the particle-field equipartition condition is $U_{\rm p}[1+(1+\chi)/\kappa] = B^2/8\pi$, so that

$$B \;=\; \left[\frac{7.44\times10^{-21}}{1+\chi}\,\Big[1+\frac{\kappa}{1+\chi}\Big]\,\frac{\gamma_1^{2-q}\,250^{q/2}\,\psi}{(q-2)\;a(q)}\right]^{\frac{2}{5+q}}\,. \tag{7}$$

Inserting Eq.(7) into Eq.(5) we get $(\frac{{\rm d}\gamma}{{\rm d}t})_{\rm syn} \propto \gamma_1^{2(9-q)/(5+q)}$. Once the value of $n_{\rm e,th}$ is specified (see Table 1), by equating Eqs.(5,6) we deduce γ_1.

The secondary-to-primary electron ratio χ, which appears in Eqs.(7), depends on the injection p/e number ratio, $r_{p/e} = (m_{\rm p}/m_{\rm e})^{(q_{\rm inj}-1)/2}$ (see Appendix), and on the gas optical thickness to p-p interactions. Proton-proton (p-p) collisions lead to the the production of charged and neutral pions. An electron is produced in the decay $\pi^- \to \mu^- + \nu_\mu + \bar{\nu}_e$ followed by $\mu^- \to e^- + \nu_\mu + \bar{\nu}_e$. Given the branching ratios in p-p collisions, only a third of these collisions produce electrons. The mean free path of CR protons in a medium of density $n_{\rm p}$ due to p-p interactions is $\lambda_{\rm pp} = (\sigma_{\rm pp}n_{\rm p})^{-1}$; for protons with kinetic energy $T \sim$ few TeV the cross section is $\sigma_{\rm pp} \simeq 50\,{\rm mb} = 5\times10^{-26}\,{\rm cm}^2$ (Baltrusaitis et al. 1984). For a typical SB ambient gas density $n_{\rm p} \simeq 150\,{\rm cm}^{-3}$, $\lambda_{\rm pp} \sim 43\,{\rm kpc}$. The probability for a single CR proton to undergo a pp interaction in its 3D random walk through a region of radius $r_{\rm s} \sim 0.25\,{\rm kpc}$ (also typical of SB nuclei) is then $\sqrt{3}\,r_{\rm s}/\lambda_{\rm pp} \simeq 0.01$. We then estimate that in typical SB environments, characterized by relatively strong non-relativistic shocks ($q_{\rm inj} = 2.2$, see Appendix), the secondary to primary electron ratio is $\chi = \chi_0\,\sqrt{3}\,(r_{\rm s}/\lambda_{\rm pp}) \simeq 0.3$. For quiescent environments, with typical values $n_{\rm p} \simeq 1\,{\rm cm}^{-3}$ and $r_{\rm s} \sim 2.5\,{\rm kpc}$, we find $\chi \simeq 0.03$. The higher value found for starbursts is in approximate agreement with results of detailed numerical starburst models for energies $\gtrsim 10\,{\rm MeV}$ (plotted in, e.g., Paglione et al. 1996; Torres 2004; Domingo-Santamaría & Torres 2005; De Cea et al. 2009; Rephaeli et al. 2010).

To compute the CR p/e energy density, κ (see Appendix), we assume power-law spectra for the CR particles: *(i)* the electron spectral index $q_{\rm e}$ is deduced from the measured synchrotron radiation index α, according to the standard formula $q_{\rm e} = 2\alpha+1$; and *(ii)* the proton spectral index is assumed to be close to the injection value, $q_{\rm p} \sim q_{\rm inj} \simeq 2.1-2.2$, for the dense, CR-producing, SB environments hosted in the central regions of some galaxies, and equal to the leaky-box value, $q_{\rm p} = q_{\rm inj} + \delta \simeq 2.7$ (where $\delta \simeq 0.5$ is the diffusion index) for more tenuous, CR-diffusing, quietly star forming galaxies. Values of κ for our sample galaxies are reported in Section 5.

Finally, we obtain an explicit expression for $U_{\rm p}$:

$$U_{\rm p} \;=\; \frac{1}{8\,\pi}\left[1+\frac{1+\chi}{\kappa}\right]^{-1}\;\times$$
$$\times\;\left[\frac{7.44\times10^{-21}}{1+\chi}\,\Big[1+\frac{\kappa}{1+\chi}\Big]\,\frac{\gamma_1^{2-q}\,250^{q/2}\,\psi}{(q-2)\;a(q)}\right]^{\frac{4}{5+q}}\,. \tag{8}$$

Table 1. Star-forming galaxies: the data.

Object	$D_L^{[1]}$ (Mpc)	$r_{\rm s}^{[2]}$ (kpc)	$f_{\rm 1\,GHz}^{[3]}$ (Jy)	$\alpha_{\rm NT}^{[4]}$	$n_{\rm e,\,th}^{[5]}$ ($\rm cm^{-3}$)	$L_{\rm TIR}^{[6]}$ (erg/s)	SFR[7] ($M_\odot$/yr)	$\nu_{\rm SN}^{[8]}$ ($\rm yr^{-1}$)	$M_{\rm gas}^{[9]}$ ($M_\odot$)	$L_\gamma^{[10]}$ (erg/s)	$\tau_{\rm res}^{[11]}$ (yr)	Notes
Arp 220	74.7	0.25	0.3	0.65	300	45.75	253	3.5	$9.24^{+0.10}_{-0.11}$	< 42.25	9.0E+3	SB
M 82	3.4	0.26	10.0	0.71	200	44.26	8.2	0.25	$9.37^{+0.09}_{-0.14}$	$40.21^{+0.10}_{-0.13}$	2.6E+3	SB
NGC 253	2.5	0.20	5.6	0.75	400	44.23	7.7	0.12	$9.20^{+0.10}_{-0.11}$	$39.76^{+0.14}_{-0.19}$	2.0E+4	SB
Milky Way	–	4.4	–	–	0.01	43.75	2.5	0.02	$9.81^{+0.12}_{-0.16}$	$38.91^{+0.12}_{-0.15}$	2.7E+7	quiescent
M 31	0.78	5.17	4.8	0.88	0.01	42.98	0.43	0.01	$9.88^{+0.11}_{-0.15}$	$38.66^{+0.09}_{-0.10}$	4.0E+7	quiescent
M 33	0.85	2.79	3.30	0.95	0.03	42.68	0.22	0.003	$9.35^{+0.13}_{-0.19}$	< 38.54	2.6E+7	quiescent
LMC	0.049	3.0	285.0	0.84	0.01	42.45	0.16	0.002	$8.86^{+0.12}_{-0.18}$	$37.67^{+0.05}_{-0.05}$	1.0E+7	quiescent
SMC	0.061	1.53	45.3	0.85	0.01	41.45	0.01	0.001	$8.66^{+0.03}_{-0.06}$	$37.04^{+0.11}_{-0.14}$	4.0E+7	quiescent
NGC 4945	3.7	0.22	5.5	0.57	300	44.02	4.7	0.1-0.5	$9.64^{+0.10}_{-0.40}$	$40.30^{+0.12}_{-0.16}$	4.6E+4	SB+Sy2
NGC 1068	16.7	1.18	6.6	0.75	300	45.05	50	0.2-0.4	$9.71^{+0.11}_{-0.19}$	$41.32^{+0.15}_{-0.23}$	1.0E+6	SB+Sy2

[1] Distance (from Abdo et al. 2011).

[2] Effective radius of star-forming region. See text. Data are from Persic & Rephaeli 2010 and refs. therein (Arp 220, M 82, NGC 253), Beck & Gräve 1982 (M 31), Tabatabaei et al. 2007 (M 33), Weinberg & Nikolaev 2001 (LMC), Wilke et al. 2003 (SMC), Moorwood & Oliva 1994 (NGC 4945), Spinoglio et al. 2005 (NGC 1068).

[3] 1 GHz flux density. Data are from Persic & Rephaeli 2010 and refs. therein (Arp 220, M 82, NGC 253)), Beck & Gräve 1982 (M 31), Tabatabaei et al. 2007 (M 33), Klein et al. 1989 (LMC), Haynes et al. 1991 (SMC), Elmouttie et al. 1997 (NGC 4945), Kühr et al. 1981 (NGC 1068).

[4] Non-thermal spectral radio index. Data are from Persic & Rephaeli 2010 and refs. therein (Arp 220, M 82, NGC 253), Beck & Gräve 1982 (M 31), Tabatabaei et al. 2007 (M 33), Klein et al. 1989 (LMC), Haynes et al. 1991 (SMC), Elmouttie et al. 1997 (NGC 4945), Kühr et al. 1981 (NGC 1068).

[5] Thermal electron density. Data are from Roy et al. 2010 (Arp 220), Petuchowski et al. 1994 (M 82), Kewley et al. 2000 and Carral et al. 1994 (NGC 253), Cox 2005 (Milky Way), Beck 2000 (M 31), Jababtabaei et al. 2008 (M 33), Points et al. 2001 (LMC), Sasaki et al. 2002 (SMC), Spoon et al. 2000 (NGC 4945), Kewley et al. 2000 (NGC 1068).

[6] Total IR [i.e., $(8-1000)\mu$m] luminosity, in log (from Abdo et al. 2011).

[7] Star formation rate, from $\mathrm{SFR} = L_{\rm IR}/(2.2 \times 10^{43}\,\mathrm{erg/s})$ (Kennicutt 1998).

[8] Core-collapse SN rate. Data are from Persic & Rephaeli 2010 and references therein (Arp 220, M 82, NGC 253), Diehl et al. 2006 (Milky Way), van den Bergh & Tammann 1991 (M 31, M 33, SMC, LMC; see also Pavlidou & Fields 2001), Lenain et al. 2010 and references therein (NGC 4945, NGC 1068). For NGC 1068 we also computed an upper limit to the SN rate ($\nu_{\rm SN} \leq 0.39$) using Mannucci et al.'s (2003) formula $\nu_{\rm SN} = (2.4 \pm 0.1) \times 10^{-2} [L_{\rm FIR}/(10^{10} L_\odot)]\,\mathrm{yr}^{-1}$, being $f_{\rm FIR} = 1.26 \times 10^{-11} (2.58\, f_{60} + f_{100})\,\mathrm{erg\,cm^{-2}s^{-1}}$ (see Helou et al. 1988) with $f_{60} \simeq 190$ Jy and $f_{100} \simeq 277$ Jy.

[9] Gas mass (neutral plus molecular hydrogen: $M_{\rm HI} + M_{\rm H_2}$), in log. Data are from: Torres 2004 for Arp 220; Abdo et al. 2010a for M 82, NGC 253, and the Milky Way; Abdo et al. 2010b for M 31 and M 33; Abdo et al. 2010c for the LMC; Abdo et al. 2010d for the SMC; and Lenain et al. 2010 for NGC 4945 and NGC 1068.

[10] High-energy (>100 MeV) γ-ray luminosity, in log (from Abdo et al. 2011).

[11] CRp residency time.

Using Eq.(8), numerical values of $U_{\rm p}$ can be obtained from the relevant observational quantities for our sample galaxies (see Table 1); these values are reported in Table 2.

3 ESTIMATING $U_{\rm P}$ FROM γ-RAY EMISSION

In this section we will review some basic features of the modeling of γ-ray emission from star-forming galaxies, and the status of HE/VHE γ-ray observations. Detections of several such galaxies have enabled measurements of $U_{\rm p}$ values either in SB cores or throughout the disk.

In most SB galaxies, such as the two nearby ones M 82 and NGC 253, the central SB region (also called the source region) with a radius of $\sim 200-300$ pc, is identified as the main site of particle acceleration. Here, the injection particle spectrum is assumed to have the non-relativistic strong-shock index $q = 2$. A theoretical $N_{\rm p}/N_{\rm e}$ ratio, predicted from charge neutrality of the injected CR, is likely to hold in this source region – as is also the assumption of equipartition. A measured radio index $\alpha \simeq 0.75$ in the source region implies $q = 2\,\alpha + 1 \simeq 2.5$ there. This indicates a substantial steepening of the CRe spectrum from the injection value $q_0 = 2$ due to diffusion ($D \propto \gamma^{-\delta}$) effects that cause the steady-state particle spectral index to be $q_0 + \delta$ above some break energy. As an example, the steady-state electron and proton spectra in the SB region of NGC 253 are shown in Fig. 1. At low energies both spectra are flatter, whereas at $E >> 1$ GeV the stronger electron losses result in steeper electron spectra.

Adopting the convection-diffusion model for energetic electron and proton propagation and accounting for all the

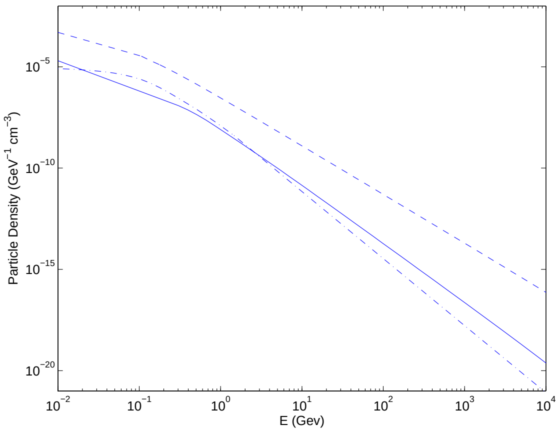

Figure 1. Properties of the emitting particles in the central SB region of NGC 253 (Rephaeli et al. 2010): steady-state spectra of primary (solid line) and secondary (dot-dashed line) electrons, and of protons (dashed line).

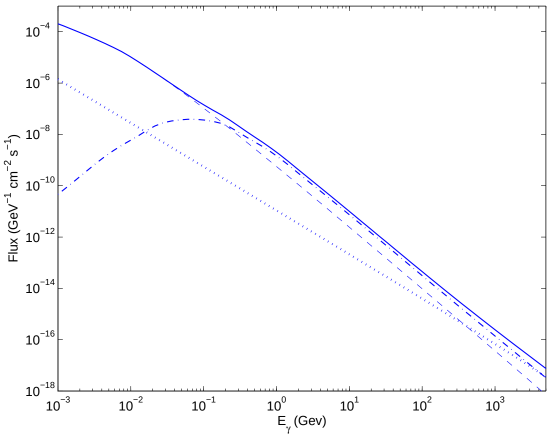

Figure 2. Properties of the emitted radiation in the central SB region of NGC 253 (Rephaeli et al. 2010): radiative yields from electron Compton scattering off the FIR radiation field (dotted line), electron bremsstrahlung off ambient protons (dashed line), π^0 decay following p-p collisions (dashed-dotted line), and their sum (solid line).

relevant hadronic and leptonic processes, the steady-state energy distributions of these particles, in both the (active) SB nucleus and the (passive) disk of these galaxies, can be determined with a detailed numerical treatment once the gas distribution is known (e.g., Torres 2004; Persic, Rephaeli & Arieli 2008; Rephaeli, Arieli & Persic 2010).

The relevant electron energy loss processes are bremsstrahlung, Compton, and synchrotron, whereas for protons the main losses are γ-ray emission from π^0 decay following p-p collisions (see Fig. 2); bremsstrahlung losses dominate at lower energies, whereas π^0-decay losses dominate at higher energies. In the GeV-TeV region, emission is mainly from p-p–induced π^0 decay.

The procedure is similar when star formation is not undergoing a burst confined to the nuclear region but occurs throughout the whole disk.

For a source with gas number density $n_{\rm gas}$, proton energy density $U_{\rm p}$, and volume V, the integrated hadronic emission from p-p–induced π^0 decay is

$$L^{[q]}_{\geq E} \;=\; \int_V g^{[q]}_{\geq E}\; n_{\rm gas}\; U_{\rm p}\; {\rm d}V \quad {\rm s}^{-1} \tag{9}$$

with the integral emissivity $g^{[\eta]}_{\geq \epsilon}$ in units of photon s^{-1}(H-atom)$^{-1}$(eV/cm^3)$^{-1}$ (Drury et al. 1994). Therefore $U_{\rm p}$ can be determined, once $L_{\geq \epsilon}$ and $n_{\rm gas}(r)$ are observationally known and the particle steady-state energy distributions have been numerically worked out by solving the convection-diffusion model for CRe and CRp propagation. By its very nature, this is a direct measurement of $U_{\rm p}$.

The two local SB galaxies M 82 and NGC 253 are the only non-AGN extragalactic sources that have so far been detected in both the GeV (Abdo et al. 2010a) and TeV (Acciari et al. 2009; Acero et al. 2009) regions. The measured fluxes and spectra of both galaxies in the two bands agree with predictions of recent numerical models in which $U_{\rm p} = \mathcal{O}(10^2)$ eV cm^{-3} in the SB nucleus. The highest-SFR galaxy in the nearby universe, Arp 220, was undetected by MAGIC (Albert et al. 2007).

HE γ-ray detections were obtained with the Large Area Telescope (LAT) on board the orbiting *Fermi* telescope for a number of low-SFR galaxies: *(i)* the Andromeda galaxy M 31 (Abdo et al. 2010b), with $U_{\rm p} \simeq 0.35$ eV cm^{-3}; *(ii)* the Large Magellanic Cloud (LMC) whose average spectrum, either with or without the bright star-forming region of 30 Doradus, yields $U_{\rm p} \simeq 0.2 - 0.3$ eV cm^{-3} (Abdo et al. 2010c); *(iii)* the Small Magellanic Cloud (SMC), whose integrated spectrum indicates that $U_{\rm p} \simeq 0.15$ eV cm^{-3} (Abdo et al. 2010d); and *(iv)* the composite SB/Seyfert-2 galaxies NGC 1068 and NGC 4945 (Lenain et al. 2010). Only flux upper limits exist for the Triangulum galaxy M 33 (Abdo et al. 2010b).

For the Milky Way, the modeling of the Galactic diffuse HE emission along the lines outlined above suggests an average $U_{\rm p} \simeq 1$ eV cm^{-3} (Strong et al. 2010; Ackermann et al. 2011). This compares with $U_{\rm p}{\sim}1$ eV cm^{-3} measured at Earth (e.g., Webber 1987), and with (6 ± 3) eV cm^{-3} in the $\sim$200 pc region of the Galactic Center, as inferred from the measured VHE γ-ray emission (based on HESS data: Aharonian et al. 2006).

The $U_{\rm p}$ values estimated from analysis of GeV-TeV observations are reported in Table 2.

4 ESTIMATING $U_{\rm P}$ FROM SN RATES

Combining the SN frequency with the residency timescale, $\tau_{\rm res}$, of CR protons that give rise to TeV emission in the star-forming region, and assuming a bona-fide value of the energy that goes into accelerating CR particles per SN event, we can obtain a second estimate of $U_{\rm p}$ that stems from the link between CR and core-collapse SN.

The value of $\tau_{\rm res}$ is determined from those of two other timescales:

(i) energy-loss timescale for p-p interactions, $\tau_{\rm pp} = (\sigma_{\rm pp} c n_{\rm p})^{-1}$ that, for protons with kinetic energy $E \gtrsim 10$ TeV for which $\sigma_{\rm pp} \simeq 50$ mb, can be written as

$$\tau_{\rm pp} \;\sim\; 2 \times 10^5 \left(\frac{n_{\rm p}}{100\,{\rm cm}^{-3}}\right)^{-1} \quad {\rm yr}\,; \tag{10}$$

(ii) CRp advection timescale, $\tau_{\rm out}$, that characterizes the

removal of CR out of the disk mid-plane region in a fast ($v_{\rm out} \sim 2500\,{\rm km\,s^{-1}}$ for M 82: Chevalier & Clegg 1985; Seaquist & Odegard 1991; Strickland & Heckman 2009) SB-driven wind, which for a homogeneous distribution of SNe within the SB nucleus of radius $r_{\rm s}$ is

$$\tau_{\rm out} \;=\; 3\times 10^{4}\, \Big(\frac{r_{\rm s}}{0.3\,{\rm kpc}}\Big)\, \Big(\frac{v_{\rm out}}{2500\,{\rm km\,s^{-1}}}\Big)^{-1}\;{\rm yr}\,. \qquad (11)$$

(Both timescales are normalized to typical SB conditions.) Thus,

$$\tau_{\rm res}^{-1} \;=\; \tau_{\rm pp}^{-1}(n_{\rm HI}) + \tau_{\rm out}^{-1}(r_{\rm s}, v_{\rm out})\,. \qquad (12)$$

During $\tau_{\rm res}$, a number $\nu_{\rm SN}\tau_{\rm res}$ of SN explode and deposit the kinetic energy of their ejecta, $E_{\rm ej} = 10^{51}$ erg per SN (Woosley & Weaver 1995), into the interstellar medium. Arguments based on the CR energy budget in the Galaxy and SN statistics suggest that a fraction $\eta \sim 0.05 - 0.1$ of this energy is available for accelerating particles (e.g., Higdon et al. 1998; Tatischeff 2008). Accordingly, we express the CRp energy density as

$$U_{\rm p} \;=\; 85\, \frac{\nu_{\rm SN}}{0.3\,{\rm yr}^{-1}}\, \frac{\tau_{\rm res}}{3\times 10^{4}\,{\rm yr}}\, \frac{\eta}{0.05}\, \frac{E_{\rm ej}}{10^{51}\,{\rm erg}}\, \Big(\frac{r_{\rm s}}{0.3\,{\rm kpc}}\Big)^{-3} \;{\rm eV\ cm^{-3}}. \qquad (13)$$

5 VALUES OF $U_{\rm P}$ IN GALAXIES

In SB galaxies star formation activity is intense in a relatively small nuclear region, in addition to quiescent, low-intensity star formation throughout the rest of the galactic disk (which is characteristic of non-SB spiral galaxies). This is the case, for example, in the nearby M 82 and NGC 253. The star formation rate in the nuclear SB region can be sufficiently high that the main contribution to the CR density comes from acceleration (by SN shocks) in this region, with radial extent $r_{\rm s}$. The rest of the disk can then be viewed as target to the diffusing CR. In non-SB spiral galaxies, e.g. the Milky Way and the Triangulum galaxy M 33, star formation proceeds throughout the disk, where both CR sources and target gas clouds are distributed; in this case, $r_{\rm s}$ is essentially the disk radius.

For the sample of galaxies detected in γ-rays with *Fermi*/LAT (see Table 1), values of $U_{\rm p}$ were deduced directly by modelling the observed γ-ray emission. Using Eq.(8) and Eq.(13), we now provide estimates of $U_{\rm p}$ from measured radio emission from CR electrons and the statistics of SN explosions.

Arp 220. The starburst activity takes place in a central molecular-gas disk of radius 480 pc and thickness 90 pc that accounts for SFR$\sim$120 $M_\odot\,{\rm yr}^{-1}$, and embeds (at a galactocentric distance of 200 pc) two extreme starburst nuclei of radii 68 pc and 110 pc that account for SFR= 50 and 35 $M_\odot\,{\rm yr}^{-1}$, respectively. This scheme, derived from Torres (2004) and using Eq. 4 of Kennicutt (1998), is consistent with the galaxy-wide IR-inferred SFR$\sim$ 225 $M_\odot\,{\rm yr}^{-1}$. For the disk alone we assume $r_{\rm s} \simeq 0.25$ kpc, $f_{1\,{\rm GHz}} \simeq 0.3$ Jy, and $\alpha \simeq 0.65$, which implies $q_{\rm e} = 2.30$, and hence $a \simeq 0.09$; assuming $q_{\rm p} = 2.2$ leads to $\kappa \simeq 38$. From Eqs.(6) and (5), and the value of $n_{e,\,{\rm th}}$ reported in Table 1, we derive $\gamma_1 = 2650$. From Eq.(8) we then obtain $B \approx 207\,\mu$G and $U_{\rm p} \approx 1027\,{\rm eV\,cm^{-3}}$ (radio method). In Eq.(11) we use 0.09 kpc, the thickness of the starburst disk perpendicular to which the wind breaks out, to compute $\tau_{\rm adv} \simeq 9\times 10^{3}$yr (being $n_p \simeq 10^{2}\,{\rm cm^{-3}}$; and using the latter and $\nu_{\rm SN} = 3.5\,{\rm yr}^{-1}$ in Eq.(13), we get $U_{\rm p} \approx 515\,{\rm eV\,cm^{-3}}$ (SN method).

M 82. Following Persic et al. (2008; and references therein) we take the central SB to be a region with a radius of 300 pc and height of 200 pc, hence $r_{\rm s} = 260$ pc, whose non-thermal radio emission has $f_{1\,{\rm GHz}} = 10$ Jy and $\alpha \simeq 0.71$. The latter implies $q \simeq 2.42$, that yields $a \simeq 0.09$; assuming $q_{\rm p} = 2.2$, we then compute $\kappa \simeq 60$. From Eqs.(6) and (5), and the value of $n_{e,\,{\rm th}}$ reported in Table 1, we derive $\gamma_1 = 4724$. From Eq.(8) we then obtain $B \approx 91\,\mu$G and $U_{\rm p} \approx 201\,{\rm eV\,cm^{-3}}$ in the SB nucleus (radio method). Because $\nu_{\rm SN} = 0.25\,{\rm yr}^{-1}$ and $\tau_{\rm res} \sim \tau_{\rm out} \simeq 3\times 10^{4}$yr (taking $n_{\rm p} \sim 10^{2}{\rm cm^{-3}}$ in the SB nucleus, and $v_{\rm out} \sim 2500$ km s^{-}1; see Persic & Rephaeli 2010), from Eq.(13) we get $U_{\rm p} \approx 95\,{\rm eV\,cm^{-3}}$ (SN method);

NGC 253. Following Rephaeli et al. (2010, and references therein) we assume $r_{\rm s} = 200$ pc, $f_{1\,{\rm GHz}} = 5.6$ Jy, and $\alpha \simeq 0.75$. The latter implies $q \simeq 2.50$, hence $a = 0.0852$; assuming $q_{\rm p} = 2.2$, we get $\kappa \simeq 76$. From Eqs.(6) and (5), and the value of $n_{e,\,{\rm th}}$ reported in Table 1, we derive $\gamma_1 = 7886$. From Eq.(8) we then obtain $B \approx 77\,\mu$G and $U_{\rm p} \approx 145\,{\rm eV\,cm^{-3}}$ in the starburst nucleus (radio method). Being $\nu_{\rm SN} = 0.12\,{\rm yr}^{-1}$ and $\tau_{\rm res} \sim \tau_{\rm out} \simeq 3\times 10^{4}$yr (being $n_{\rm p} \sim 10^{2}$ cm^{-3}, in the starburst nucleus, and $v_{\rm out} \sim 2500$ km s^{-}1; see Persic & Rephaeli 2010), we get $U_{\rm p} \approx 75\,{\rm eV\,cm^{-3}}$ (SN method);

Milky Way. Measurements of Galactic CR indicate $U_{\rm p} \simeq$ 1 eV at the Sun's position. The Galactic CRp flux measured locally is the result of the superposition of particles, accelerated in several sites scattered throughout the Galaxy, that have diffused out into the disk. Accordingly, we view the entire Galaxy as the region where SN occur, and adopt 15 kpc and a thickness of 0.5 kpc, so that $r_{\rm s} = 4.4$ kpc, $\tau_{\rm res} \sim 2\times 10^{7}$ yr (with $n_{\rm p} \sim 1\,{\rm cm^{-3}}$), and $\nu_{\rm SN} = 0.02\,{\rm yr}^{-1}$, leading to $U_{\rm p} \approx 1\,{\rm eV\,cm^{-3}}$ (SN method). Alternatively, if we directly compare our SN-based estimate to available measurements of the innermost Galactic region, we need to estimate the relevant quantities in a nuclear region with $r_{\rm s} = 0.2$ kpc. The most prominent large-scale distribution of HI gas in the Galaxy is an exponential disk with $R_d = 3.75$ kpc coplanar to the stellar disk with $n_{\rm HI} = 1\,{\rm cm^{-3}}$ in the solar neighborhood, i.e. at a Galactocentric distance $R_0 = 8$ kpc (Dehnen & Binney 1998): this implies that the average density within $r_{\rm s}$ is $\bar{n}_{\rm HI} \simeq 8\,{\rm cm^{-3}}$, hence $\tau_{\rm pp} = 2.5\times 10^{6}$ yr there. The full disk Galactic SN rate, $\nu_{\rm SN} = 0.02\,{\rm yr}^{-1}$ (Diehl et al. 2006), should similarly be rescaled to the $r_{\rm s}$ region: In an exponential disk with $R_d = 2.5$ kpc (Dehnen & Binney 1998), $r_{\rm s}$ contains 0.3% of the total mass; consequently, $\nu_{\rm SN} = 0.6\times 10^{-4}\,{\rm yr}^{-1}$, leading to $U_{\rm p} \approx 5\,{\rm eV\,cm^{-3}}$ (SN method).

M 31. With an average value of the spectral index, $\alpha = 0.88$, and the (nonthermal) flux (at 2.7 GHz) reported by Beck & Gräve (1982), we deduce $f_{1\,{\rm GHz}} = 4.8$ Jy, averaged over 19.2 kpc radius. The latter corresponds to $\sim$3.34 exponential length scales ($R_d = 5.75$ kpc, averaging VRI data from Hou et al. 2009), i.e. the corresponding volume encloses $\sim$85% of the mass of the exponential disk, hence most of the stellar distribution. With an assumed thickness of 0.5 kpc, we get $r_{\rm s} = 5.17$ kpc. The measured spectral radio index implies $q =$ 2.76, and $a \simeq 0.08$; assuming $q_{\rm p} = 2.7$, we get $\kappa \simeq 8$. From Eqs.(6) and (5), and the value of $n_{e,\,{\rm th}}$ reported in Table 1, we derive $\gamma_1 = 1169$, and from Eq.(8) we then obtain $B \approx$

$2.6\,\mu$G and $U_{\rm p} \approx 0.15\,{\rm eV\,cm^{-3}}$ (radio method). Taking the whole disk as a site for SN explosions, the implied average gas density is $n_{\rm p} \simeq 0.5\,{\rm cm^{-3}}$, hence $\tau_{\rm res} \sim \tau_{\rm pp} \simeq 3.7 \times 10^7$yr. Eq.(13) then yields $U_{\rm p} \approx 0.2\,{\rm eV\,cm^{-3}}$ (SN method).

M 33. Star formation - traced by OB associations and HII regions (e.g., Bastian et al. 2007) - and SN occur throughout the disk. From Tabatabaei et al. (2007) we derive a non-thermal radio flux $f_{1\,{\rm GHz}} = 3.3$ Jy and $\alpha = 0.95$, averaged over 7.6 kpc radius. The latter corresponds to 5.3 exponential lengthscales ($R_d \simeq 1.43$ kpc, from Regan & Vogel 1994), enclosing 97% of the mass of an exponential disk, hence virtually the whole stellar distribution. For an assumed thickness of 0.5 kpc, we get $r_{\rm s} = 2.79$ kpc. The measured spectral index implies $q = 2.90$, and $a \simeq 0.08$; assuming $q_{\rm p} = 2.7$, we get $\kappa \simeq 11.2$. From Eqs.(6) and (5), and the value of $n_{e,\,\rm th}$ reported in Table 1, we derive $\gamma_1 = 1287$. From Eq.(8) we then obtain $B \approx 4.1\,\mu$G and $U_{\rm p} \approx 0.38\,{\rm eV\,cm^{-3}}$ (radio method). Given the gas mass reported in Table 1, the average gas density is $n_{\rm p} \sim 1\,{\rm cm^{-3}}$, hence $\tau_{\rm res} \sim \tau_{\rm pp} \simeq 2 \times 10^7$yr. Inserting the relevant quantities (see Table 1) into Eq.(13), we then derive $U_{\rm p} \approx 0.7\,{\rm eV\,cm^{-3}}$ (SN method).

LMC. This satellite of the Milky Way can be modeled as a truncated disk/spheroid with $r_{\rm t} \simeq 3$ kpc whose half-thickness is also $\simeq$3 kpc (Weinberg & Nikolaev 2001), so we use $r_{\rm s} = 3$ kpc in Eqs.(13,8). The measured spectral radio index implies $q = 2.68$, and $a \simeq 0.08$; assuming $q_{\rm p} = 2.7$, we get $\kappa \simeq 6.7$. From Eqs.(6) and (5), and the value of $n_{e,\,\rm th}$ reported in Table 1, we derive $\gamma_1 = 1189$. Eq.(8) then yields $B \approx 2.6\,\mu$G and $U_{\rm p} \approx 0.14\,{\rm eV\,cm^{-3}}$ (radio method). There is no mass outflow in the LMC, hence $\tau_{\rm res} \sim \tau_{\rm pp} \approx 10^7$yr (using an average gas density of $n_{\rm p} \approx 2\,{\rm cm^{-3}}$.) Eq.(13) then yields $U_{\rm p} \approx 0.2\,{\rm eV\,cm^{-3}}$ (SN method).

SMC. This other Milky Way satellite can be modeled as a bar with an area $\simeq 2.5 \times 1.5$ kpc (Wilke et al. 2003) and l.o.s. extent of 4 kpc (following Abdo et al. 2010d), so we use $r_{\rm s} = 1.53$ kpc in Eqs.(13,8). The measured radio spectral index implies $q = 2.70$, and $a \simeq 0.08$; assuming $q_{\rm p} = 2.7$, we get $\kappa \simeq 20$. From Eqs.(6) and (5), and the value of $n_{e,\,\rm th}$ reported in Table 1, we derive $\gamma_1 = 754$. From Eq.(8) we obtain $B \approx 4\,\mu$G and $U_{\rm p} \approx 0.39\,{\rm eV\,cm^{-3}}$ (radio method). The SMC has a (galaxy-wide) SN rate of $\nu_{\rm SN} = 10^{-3}\,{\rm yr^{-1}}$. There is no mass outflow from the SMC, so $\tau_{\rm res} \sim \tau_{\rm pp} \simeq 1.4 \times 10^7$yr. (It is $n_{\rm p} \simeq 1.4\,{\rm cm^{-3}}$.) From Eq.(13) we then obtain $U_{\rm p} \approx 1\,{\rm eV\,cm^{-3}}$ (SN method).

NGC 4945. This almost edge-on galaxy hosts a Seyfert-2 nucleus (deduced from its X-ray variability, Iwasawa et al. 1993). However, essentially all its IR radiation arises from a central $33'' \times 19''$ ($r_{\rm s} = 0.22$ kpc) molecular complex whose IR colors are typical of SB activity (see Moorwood & Oliva 1994). The measured nuclear radio emission implies $q = 2.14$, and $a \simeq 0.10$; assuming $q_{\rm p} = 2.2$, we get $\kappa \simeq 15.7$. From Eqs.(6) and (5), and the value of $n_{e,\,\rm th}$ reported in Table 1, we derive $\gamma_1 = 5689$. Assuming the measured radio flux to be only related to the SB, from Eq.(8) we then get $B \approx 94\,\mu$G and $U_{\rm p} \approx 201\,{\rm eV\,cm^{-3}}$ (radio method). It follows from $\nu_{\rm SN} \sim 0.2\,{\rm yr^{-1}}$, and the existence of a galactic wind with $v_{\rm out} \sim 1200\ {\rm km\,s^{-1}}$ (Chen & Huang 1997) that $\tau_{\rm res} \sim \tau_{\rm out} \simeq 4.6 \times 10^4$ yr; Eq.(13) then yields $U_{\rm p} \approx 220\,{\rm eV\,cm^{-3}}$ (SN method);

NGC 1068. This galaxy hosts a prototypical Seyfert-2 nucleus (e.g., Wilson & Ulvestad 1982). The circumnuclear SB region can be modeled as a spherical shell with external radius of 1.5 kpc and thickness 0.3 kpc, and mass $3.4 \times 10^9 M_\odot$ (Spinoglio et al. 2005). The effective radius is then $r_{\rm s} = 1.2$ kpc, and the average density is $n_{\rm p} \sim 20\,{\rm cm^{-3}}$. The measured spectral index implies $q \simeq 2.50$, hence $a = 0.0852$ – assuming $q_{\rm p} = 2.2$, we get $\kappa \simeq 76$. From Eqs.(6) and (5), and the value of $n_{e,\,\rm th}$ reported in Table 1, we derive $\gamma_1 = 10161$, and from Eq.(8) we then compute $B \approx 52\,\mu$G and $U_{\rm p} \approx 65\,{\rm eV\,cm^{-3}}$ (radio method). The CRp residency time is $\tau_{\rm res} \sim \tau_{\rm pp} \simeq 10^6$yr. (The outgoing wind observed in NGC 1068 does not emanate from the SB region, but from close to the central AGN, see Krolik & Begelman 1986.) Assuming all the observed far-IR emission originates from the SB region, yields $\nu_{\rm SN} = 0.39\,{\rm yr^{-1}}$ there (see Table 1). Inserting the relevant quantities into Eq.(13) we get $B \approx 52\,\mu$G and $U_{\rm p} \approx 65\,{\rm eV\,cm^{-3}}$ (SN method).

Table 2. Star-forming galaxies: CRp energy densities$^+$.

Object	γ-ray meth.	radio meth.	SN meth.	other meth.	$r_{\rm s}$ (kpc)	loss mode
Arp 220	–	1027	515	–	0.25	adv
M 82	$200^{\rm a,c}$	201	95	–	0.26	adv
NGC 253	$200^{\rm b,c}$	145	77	–	0.20	adv
Milky Way	$1^{\rm d}$	–	1	$1^{\rm j}$	4.4	pp
	$6^{\rm e}$	–	5	–	0.2	pp
M 31	$0.36^{\rm f}$	0.15	0.7	–	4.77	pp
M 33	$< 3^{\rm f}$	0.38	0.7	–	2.79	pp
LMC	$0.25^{\rm g}$	0.14	0.2	–	3.0	pp
SMC	$0.15^{\rm h}$	0.39	1.0	–	1.53	pp
NGC 4945	$200^{\rm i}$	201	220	–	0.22	adv
NGC 1068	–	65	61	–	1.18	pp

$^+$ Values are in ${\rm eV\,cm^{-3}}$.

(a) Acciari et al. 2009 (see also Persic et al. 2008 and De Cea et al. 2009). *(b)* Acero et al. 2009 (see also Paglione et al. 1996, Domingo-Santamaría & Torres 2005, and Rephaeli et al. 2010). *(c)* Abdo et al. 2010a. *(d)* Strong et al. 2010. *(e)* Aharonian et al. 2006. *(f)* Abdo et al. 2010b, with Drury et al. 1994 in the case of M 33. *(g)* Abdo et al. 2010c. *(h)* Abdo et al. 2010d. *(i)* Lenain et al. 2010. *(j)* Webber 1987.

5.1 Uncertainties

The values of $U_{\rm p}$ listed in Table 2 do not include substantial observational and modeling uncertainties. In this section we attempt to estimate the level of precision with which $U_{\rm p}$ was determined based on only limited information on the errors in the various observational parameters.

5.1.1 Radio Method

The quantities in Eq.(8) are usually well determined for our sample galaxies, except for the p/e energy density ratio κ, for which a CRp spectral index, $q_{\rm p}$, must be assumed. Given its possible values discussed in the Appendix (i.e., $q_{\rm p} \simeq 2.1-2.2$ in SB regions, and $q_{\rm p} \simeq 2.1-2.2$ for quiescent galaxies), the uncertainty on the CRp spectral index, $\delta q_{\rm p} \simeq 0.1$, translates to a factor of $\sim$2 uncertainty on κ [see Eq.(24)], i.e. typically an uncertainty of $\sim$50% on $U_{\rm p}$ as deduced from Eq.(8).

We emphasize that the use of κ here is slightly different from that of Persic & Rephaeli (2010), where we assumed $q_{\rm p} = q_{\rm e} = 2\alpha + 1$ in all galaxies, whereas here we appropriately drop such equality and assume a physically motivated index, separately for SB ($q_{\rm p} \simeq\neq q_{\rm inj}$) and quiescent ($q_{\rm p} \simeq\neq q_{\rm inj} + \delta$) galaxies. Numerically the values of $q_{\rm p}$ assumed here are not that different from the measured $q_{\rm e}$.

Another improvement in the present radio-based derivation of $U_{\rm p}$ relates to the electron low-energy cutoff, γ_1. In Persic & Rephaeli (2010) we assumed $\gamma_1 = 10^3$, whereas here we calculate γ_1 self-consistently by setting it equal to the energy at which synchrotron and Coulomb losses are equal. Effectively then, γ_1 is the low-energy limit of the electron PL spectrum (see Eq.1).

5.1.2 Supernova Method

A precise measurement of the actual rate of core-collapse SNe is, of course, crucial in these estimates. This is quite difficult given the typically heavy optical extinction (e.g., in SB nuclei). For example, from Table 2 notice that for our SB nuclei the SN-based $U_{\rm p}$ are systematically lower, by a factor of 2, than the corresponding radio and γ estimate, whereas there is no such discrepancy in the quiescent sample. This mismatch does suggest the possibility of missing about half of the SN remnants hosted in dense, dusty environments. In addition, SN rates, even when quoted for individual galaxies, are often only statistical in nature and based on the morphology and stellar mass of the respective galaxies (e.g., Mannucci et al. 2005), especially so at low luminosities where the SN rate is very low. Finally, radio counts of SN remnants require information on their ages in order to be turned into actual SN rates. For our sample galaxies, published observational results suggest that $\nu_{\rm SN}$ are known to within a factor $\sim$2.

Also from Eq.(13) we see that uncertainties on $U_{\rm p}$ can also be due to uncertainties in $\tau_{\rm res}$. The latter mostly arise from the uncertainty in the fast wind velocity, which in turn is probably known to within a factor of $\sim$2. Estimates of the SN energy that is channeled to CR, $\sim (0.5-1)\,10^{50}$ erg, i.e. $\sim$5% − 10% of the total kinetic energy of the SN ejecta (Woosley & Weaver 1995), agree within a factor $\lesssim 2$ (Lingenfelter et al. 1998; Higdon et al. 1998). (Here we assume that all core-collapse SN share a universal CR acceleration efficiency.)

Finally, for all our sample galaxies, the effective star-forming radii $r_{\rm s}$ are deduced from high-resolution optical and radio data, so their values are relatively precise, with typical uncertainties of a few 10%.

We conclude that all the galaxy quantities in Table 1 relevant to Eq.(13) are quoted in the literature as observationally precise to within a factor of $\lesssim 2$, so that $U_{\rm p}$ can only be estimated from Eq.(13) to within a factor $\sim$4.

6 DISCUSSION

The three methods discussed here are not independent. The γ-ray method and the radio method are coupled through the p/e ratio at injection, through the secondary-to-primary electron ratio, and through the imposed condition of particle-field equipartition. The SN method is not independent of the γ-ray method either, because both depend on the residency time of CRp in the emission region - although, unlike the γ-ray and radio methods, it does not depend on the particle radiative yield but on the statistics of core-collapse SN. Also, the γ-ray, radio, and SN methods are not on equal footing. By these methods the value of $U_{\rm p}$ is either *measured*, *inferred*, or *estimated*, respectively. This, because: *(i)* π^0-decay γ-ray emission is the most robust *measure* of $U_{\rm p}$ when the distribution of target gas is known and the particle diffusion mode and energy losses are accurately known, whereas *(ii)* radio emission enables *deduction* of $U_{\rm p}$ from electron synchrotron flux and spectrum once assumptions have been made on the link between energetic electrons and protons, and between these particles and the magnetic field; and *(iii)* assuming a SN origin for CR, SN statistics for a given (region of a) galaxy leads to an *estimate* of $U_{\rm p}$ there.

A substantial agreement among estimates based on the three methods is reached for most of the galaxies in Table 1. The only exceptions are *(a)* the SMC and *(b)* the SB/Seyfert-2 galaxy NGC 1068. Possible reasons for these discrepancies are:

(a) The SMC mean magnetic field might be sufficiently weak that there is only a partial CR confinement, so that most CR diffuse out to the intergalactic space (Abdo et al. 2010d). If so, the radio method yields the (lower) *actual* particle energy density, whereas the SN method gives an estimate of the (higher) *produced* amount.

(b) Unlike for NGC 4945 (the other SB/Seyfert-2 galaxy in our sample), the spectral energy distribution of NGC 1068 differs markedly from that of purely SB galaxies, suggesting that its γ-ray emission may be unrelated to star formation (Lenain et al. 2010). Indications that this may be the case are that *(i)* there is no galactic wind emanating from the SB region of NGC 1068 (unlike all other SB galaxies in Table 1), and *(ii)* its location in the diagnostic f_{12}/f_{25} vs. f_{60}/f_{100} plane [1] (see Persic & Rephaeli 2007 and references therein) suggests that NGC 1068 does not behave as a typical SB galaxy. (Its colors suggest an 'evolved starburst phase', in which star formation activity has decreased dramatically from the SB peak, and cirrus emission, which is unrelated to ongoing star formation activity, apparently contributes strongly to the IR emission.) Finally, NGC 1068 does not conform with the trend set by the other star-forming galaxies in Table 1, in the $L(>100\,{\rm MeV})$ vs. $\nu_{\rm SN}\times M_{\rm gas}$ plane (Fig. 3*d*) and the $L(>100\,{\rm MeV})$ vs. $\nu_{\rm SN}$ plane (Fig. 3*e*; see also Lenain et al. 2010). The discrepancy is even larger if the true $\nu_{\rm SN}$ is significantly lower then the value reported in Table 1 and used in Fig. 3 (as it would be if derived from the SB-only component of the circumnuclear IR emission).

Once these considerations are weighed in, the discrepancy between the very high CRp energy densities ($U_{\rm p} \sim \mathcal{O}(10^2)\,{\rm eV\,cm^{-3}}$), deduced for SB nuclei, and the low values ($U_{\rm p} \sim \mathcal{O}(10^{-1})\,{\rm eV\,cm^{-3}}$), deduced for very quiet environments, appears very significant.

Observationally, the link between HE γ-ray emission and SNe is displayed in Fig. 3 for our sample galaxies. The

---

[1] The *IRAS* flux densities of NGC 1068 at 12, 25, 60 and 100μm are $f_{12} = 38.7$, $f_{25} = 87.4$, $f_{60} = 190$, $f_{100} = 277$.

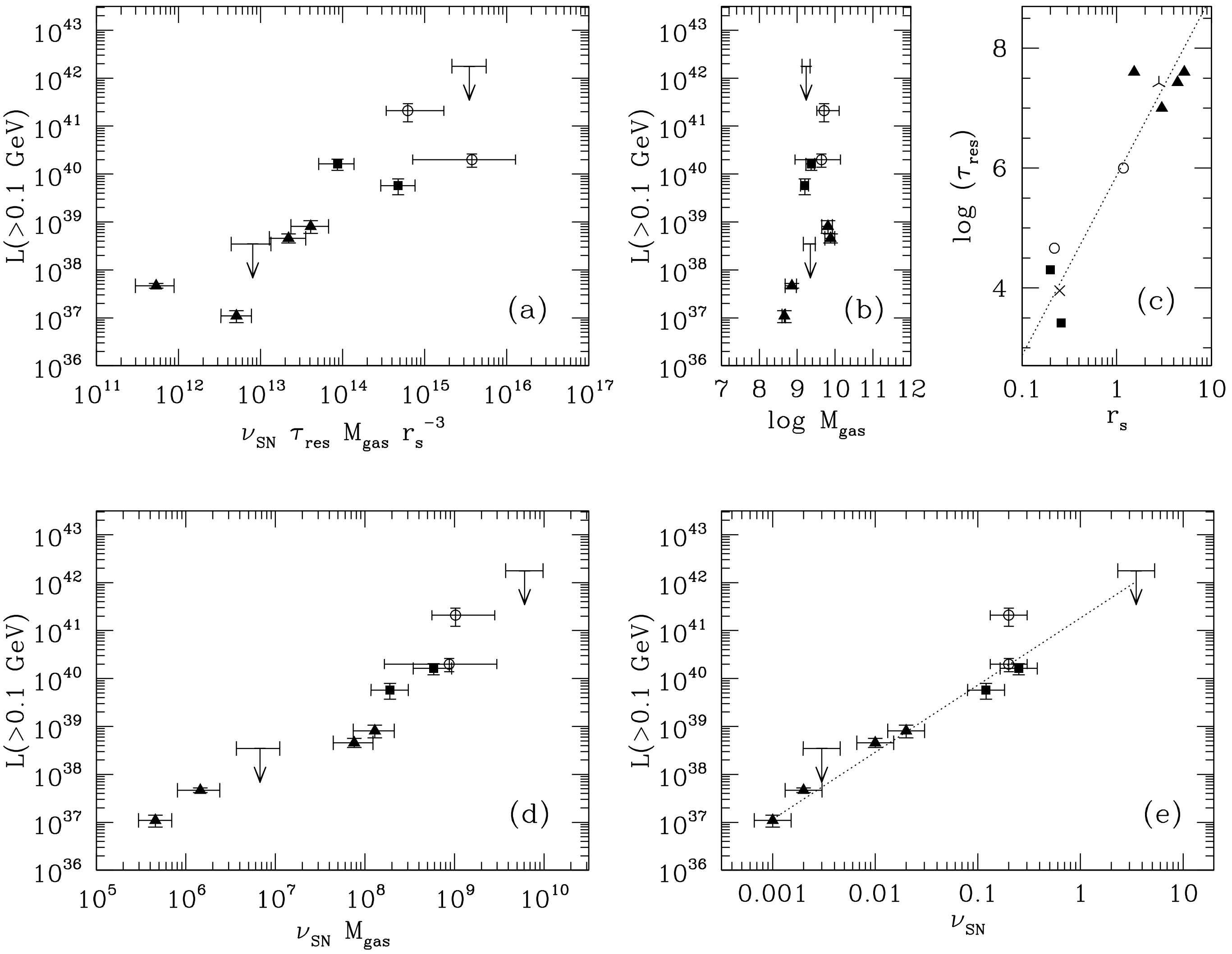

Figure 3. Correlations for all the star-forming galaxies detected by *Fermi*/LAT and reported in Table 1 (empty circles: starburst/Seyfert-2 galaxies; filled squares: starburst galaxies; filled triangles: quiescent galaxies. Arrows indicate HE γ-ray flux upper limits: Arp 220 and M 33 at, respectively, higher and lower flux limits.) The Milky Way luminosity has theoretical uncertainties stemming from the range of possible emission models matching the Galactic diffuse γ-ray background (see Strong et al. 2010). Wherever plotted, SN rates are displayed with a factor of 1.5 uncertainty (see text), except for NGC 4945 and NGC 1068 where the actual range of deduced values is reported in Table 1. *(a)* Correlation between γ-ray luminosity, SN rate within the region of radius r_s under study, CRp residency time, and total gas mass. *(b)* Distribution of gas mass as a function of luminosity. *(c)* Distribution of residency time as a function of source size. To guide the reader's eye, the dotted line drawn through the data represents the $\tau_{\rm res} \propto r_{\rm s}^3$ relationship. *(d)* Correlation between γ-ray luminosity, SN rate, and total gas mass. *(e)* Correlation between γ-ray luminosity and SN rate. For comparison, the dotted line drawn through the data shows the $\nu_{\rm SN}^{1.4}$ slope, implied by the observational $L \propto {\rm SFR}^{1.4}$ relationship reported by Abdo et al. (2010b).

theoretical link is apparent from combining Eqs.(9,13)

$$L \ \propto \ \nu_{\rm SN}\ \tau_{\rm res}\ r_{\rm s}^{-3}\ M_{\rm gas}\,. \qquad (14)$$

In deriving Eq.(14) we considered that the volume-averaged γ-ray emissivities of the sample galaxies, appearing in Eq.(9), vary little from galaxy to galaxy. This is due to the relatively uniform GeV-TeV photon slopes, and corresponding CRp spectral slopes, observed for these galaxies (Abdo et al. 2011). Panel *(a)* shows the observational correlation between γ-ray luminosity, SN rate within r_s, CRp residency time, and total gas mass; the plot shows the relation expressed in Eq.(14). Can it be reduced to fewer parameters? It can, for example, if $\tau_{\rm res} \propto r_{\rm s}^3$; observationally, this latter correlation roughly holds for our sample (see panel *(b)*). A possible reason for this: if in most galaxies in the sample the CRp energy loss is dominated by p-p interactions, so $\tau_{\rm res} \sim \tau_{\rm pp} \propto n^{-1}$, and $M_{\rm gas}$ is roughly constant within the sample, so $n \propto r_{\rm s}^{-3}$, then $\tau_{\rm res} \propto r_{\rm s}^3$ follows. Indeed, in most of our galaxies the CRp energy losses are dominated by p-p interactions (see Table 2) and the gas mass varies relatively little (a decade) within the sample (see panel *(c)*). Panel *(d)* shows the 'reduced' relationship between γ-ray luminosity, SN rate, and total gas mass. A further step from Eq.(14), by taking into account that $M_{\rm gas}$ is relatively constant across the sample, is represented by panel *(e)* that shows the γ-ray luminosity - SN rate relation; note that the distribution of data points is compatible with a $\nu_{\rm SN}^{1.4}$ slope, which follows from $\nu_{\rm SN} \propto$ SFR and the observational $L_\gamma \propto {\rm SFR}^{1.4}$ relation found by Abdo et al. (2010b) for this same sample of galaxies (except the composite SB/AGN sources).

It should be noted that the steps leading from panel a through panel d to panel e are based on the relative constancy of $M_{\rm gas}$ within the sample; however, this is a clear selection effect stemming from the fact that $L(>100\,{\rm MeV})$ is higher for a larger $M_{\rm gas}$, because star formation is higher and because there is more target gas available for p-p interaction. Given the low fluxes emitted by star-forming galaxies, which are close to the sensitivities of the *Fermi*/LAT and Cherenkov instruments, it is clear that only the brightest galaxies can be observed, i.e., the most gas-rich ones, with $\log M_{\rm HI} \sim 9-10$ (see the HI mass function of galaxies, e.g. Zwaan et al. 2003).

With the exception of (the mostly Seyfert-2 galaxy) NGC 1068, current measurements of the galaxies in our sample provide appreciable evidence for the direct link between SN and VHE γ-ray emission.

7 CONCLUSION

Active star formation in galaxies leads to production of CR protons and electrons via the Fermi-I diffusive shock acceleration mechanism in SN remnants. Basic considerations suggest that the timescales required for CRp to be Fermi-I accelerated (τ_+) and to lose energy via pion decay into photons and e^+e^- pairs or via advection by bulk outflows (τ_-), are shorter than the timescale of starburst activity in galaxies ($\tau_{\rm SB}$); the latter is itself comparable with the dynamical timescale of galaxies. A consequence is that in a SB region a balance can roughly be achieved between energy gains and losses of CR during a typical burst of star formation. Under equilibrium conditions in a galaxy, a minimum-energy configuration of the field and the CR may be attained. This implies that energy densities of particles and magnetic fields may be in approximate equipartition.

For 10 galaxies for which pointed GeV-TeV data are available (from *Fermi*/LAT) and from Cherenkov telescopes), we have estimated $U_{\rm p}$ using the the radio, γ-ray, and SN methods. A substantial agreement among estimates based on the three methods is reached for 9 of the 11 galactic regions (3 SB nuclei, the Milky Way's disk and central region, 4 quiescent galaxies, 2 SB/Seyfert-2 galaxies) considered in this paper. The discrepancy between the very high values ($U_{\rm p} \sim \mathcal{O}(10^2)\,{\rm eV\,cm^{-3}}$) found in SB nuclei such as M 82, NGC 253 and NGC 4945, and the low values ($U_{\rm p} \sim \mathcal{O}(10^{-1})\,{\rm eV\,cm^{-3}}$) found in very quiet environments such as the Local Group galaxies, appears to be highly significant.

The results of this study extend the validity of our previous suggestions that:

(i) CRp energy densities in star-forming galaxies range from $\mathcal{O}(10^2)\,{\rm eV\,cm^{-3}}$ in very active environments (e.g., SB nuclei) down to $\mathcal{O}(10^{-1})\,{\rm eV\,cm^{-3}}$ in very quiet ones (e.g., Local Group galaxies);

(ii) CR energy densities and magnetic fields, inferred from radio data under the assumption of energy equipartition, can be used as proxies of the actual quantities that are measured directly only from γ-rays. This could be particularly useful in the case of distant galaxies, whose (unbeamed) γ-ray fluxes are too faint to be measured;

(iii) core-collapse SN, both in quiescent galaxies and in SB galaxies, are likely to share a universal CR acceleration efficiency; and

(iv) the Fermi-I acceleration mechanism, assumed to be at play in the environment of SN remnants, leads to acceleration timescales for CRp in galaxies such that particles and fields attain equilibrium over typical star formation timescales, in agreement with observational evidence.

Acknowledgements. This paper has developed out of a talk presented by MP at the "Beamed and Unbeamed Gamma-Rays from Galaxies" workshop (Muonio, Finland: April 11-15, 2011). MP acknowledges useful exchanges with Keith Bechtold, Jean-Philippe Lenain, Andrew Strong, and Massimo Turatto.

REFERENCES

Abdo A.A., et al. (LAT Collab.) 2011, ApJ, in preparation
Abdo A.A., et al. (LAT Collab.) 2010b, A&A, 523, L2
Abdo A.A., et al. (LAT Collab.) 2010c, A&A, 512, A7
Abdo A.A., et al. (LAT Collab.) 2010a, ApJL, 709, L152
Abdo A.A., et al. (LAT Collab.) 2010d, A&A, 523, A46
Acciari V.A., et al. (VERITAS Collab.) 2009, Nature, 462, 770
Acero F. et al. (HESS Collab.) 2009 Science, 326, 1080
Ackermann M et al. (LAT Collab.) 2011, ApJ, 726:81
Aharonian F., et al. (HESS Collab.) 2006, A&A, 449, 223
Aharonian F., et al. (HESS Collab.) 2006, Nature, 439, 695
Albert J. et al. (MAGIC Collab.) 2007, ApJ, 658, 245
Baltrusaitis R.M., et al. 1984, PRL, 52, 1380
Bastian N., Ercolano B., Gieles M., et al. 2007, MNRAS, 379, 1302
Bauer M., Pietsch W., Trinchieri G., et al. 2007, A&A, 467, 979
Beck R. 2000, in "The Interstellar Medium of M 31 and M 33", eds. E.M.Berkhuijsen, R.Beck, R.A.M.Walterbos (Aachen: Shaker), p.171 (astro-ph/0009455)
Beck R., Gräve R. 1982, A&A, 105, 192
Beck R., Krause M., 2005, Astr. Nacht., 326, 414
Bell A.R. 1978, MNRAS 182, 443
Chen Y., & Huang J.-H. 1997, ApJ, 479, L23
Chevalier R.A., Clegg A.W., 1985, Nature, 317, 44
Corral P., Hollenbach D.J., Lord S.D., et al. 1994, ApJ, 423, 223
Cox D.P. 2005, ARA&A, 43, 337
de Cea Del Pozo E., Torres D.F., Rodriguez Marrero A.Y., 2009, ApJ, 698, 1054
Dehnen W., Binney J., 1998, MNRAS, 294, 129
Diehl R., Halloin H., Kretschmer K., et al., 2006, Nature, 439, 45
Domingo-Santamaría E., Torres D.F., 2005, A&A, 444, 403
Drury L.O'C., Aharonian F.A., Völk H.J. 1994, A&A, 287, 959
Elmouttie M., Haynes R.F., Jones, K.L., et al. 1997, MNRAS, 284, 830
Fermi E. 1954, ApJ, 119, 1
Ginzburg V.L., Syrovatskii S.I., 1964, The Origin of Cosmic Rays (New York: Macmillan)
Gupta M., Webber W.R. 1989, ApJ, 340, 1124
Haynes R.F., Klein U., Wayte S.R., et al. 1991, A&A, 252, 475
Helou G., Khan I.R., Malek L., Boehmer L. 1988, ApJS, 68, 151
Higdon J.C., Lingenfelter R.E., Ramaty R., 1998, ApJ, 509, L33

Hou J., Yin J., Boissier S. et al., 2009, in Proc. of 'The Galaxy Disk in Cosmological Context', eds. J.Andersen et al. (Cambridge: Cambridge University Press), IAU Symposium Vol. 254, p.27

Hughes A., Staveley-Smith L., Kim S., Wolleben M., Filipovic, M. 2007, MNRAS, 382, 543

Iwasawa K., Koyama K., Awaki H., et al. 1993, ApJ, 409, 155

Kennicutt R.C. Jr., 1998, ARAA, 36, 189

Kewley L.J., Heisler C.A., Dopita M.A., et al. 2000, ApJ, 530, 704

Klein U., Wielebinski R., Haynes R.F., Malin D.F., 1989, A&A, 211, 280

Krolik J.H., Begelman M.C. 1986, ApJ, 308, L55

Kühr H., Witzel A., Pauliny-Toth I.I.K., Nauber U. 1981, A&AS, 45, 367

Lenain J.-P., Ricci C., Türler M., Dorner D., Walter R. 2010, A&A, 524, 72L

Lingenfelter R.E., Ramaty R., Kozlovsky B. 1998, ApJ, 500, L153

Longair M.S., 1994, High Energy Astrophysics (2nd ed.; Cambridge: Cambridge Univ. Press)

Mannucci F., Della Valle M., Panagia N., et al. 2005, A&A, 433, 807

Mannucci F., Maiolino R., Cresci G., et al. 2003, A&A, 401, 519

Moorwood A.F.M. & Oliva E. 1994, Apj, 429, 602

Paglione T.A.D., Marscher A.P., Jackson J.M., Bertsch D.L., 1996, ApJ, 460, 295

Pavlidou V., Fields B.D. 2001, ApJ, 558, 63

Persic M., Rephaeli Y., 2007, A&A, 463, 481

Persic M., Rephaeli Y. 2010, MNRAS, 403, 1569

Persic M., Rephaeli Y., Arieli Y., 2008, A&A, 486, 143

Petuchowski SJ, Bennett CL, Haas MR, et al. 1994, ApJ, 427, L17

Points S.D., Chu Y.-H., Snowden S.L., Smith R.C. 2001, ApJS, 136, 99

Protheroe R.J., Clay R.W. 2004, PASA, 21, 1

Regan M.W., Vogel. S.N. 1994, ApJ, 434, 536

Rephaeli Y., 1979, ApJ, 227, 364

Rephaeli Y., Arieli Y., Persic M. 2010, MNRAS, 401, 473

Roy A.L., Oosterloo T., Goss W.M., Anantharamaiah K.R. 2010, A&A, 517, A82

Sarazin C.L., 1999, ApJ, 520, 529

Spoon H.W.W., Koornneef J., Moorwood A.F.M., Lutz D., Tielens A.G.G.M. 2000, A&A, 357, 3000

Tabatabaei F.S., Krause M., Fletcher A., Beck R. 2008, A&A, 490, 1005

Schlickeiser R., 2002, Cosmic Ray Astrophysics (Berlin: Springer), p.472

Seaquist E.R., Odegard N., 1991, ApJ, 369, 320

Spinoglio L., Malkan M.A., Smith H.A., et al. 2005, ApJ, 623, 123

Strickland D.K., Heckman T.M., 2009, ApJ, 697, 2030

Strong A.W., Porter T.A., Digel S.W., et al. 2010, ApJ, 722, L58

Tabatabaei F.S., Beck R., Krügel E., et al. 2007, A&A, 475, 133

Tatischeff V., 2008, in "Supernovae: lights in the darkness" (XXIII Trobades Cientifiques de la Mediterrania), PoS(028) (arXiv:0804.1004)

Torres D.F., 2004, ApJ, 617, 966

Tucker W., 1975, Radiation Processes in Astrophysics (Cambridge, MA: MIT Press)

van den Bergh S., Tammann G.A., 1991, ARAA, 29, 363

Völk H.J., Klein U., Wielebinski R., 1989, A&A, 213, L12

Webber W.R. 1987, A&A, 179, 277

Weinberg M.D., Nikolaev S. 2001, ApJ, 548, 712

Wilke K., Stickel M., Haas M., et al. 2003, A&A, 401, 873

Wilson A.S., Ulvestad J.S. 1982, ApJ, 263, 576

Woosley S.E., Weaver T.A., 1995, ApJS, 101, 181

Zwaan M.A., Staveley-Smith L., Koribalski B.S., et al. 2003, AJ, 125, 2842

APPENDIX: PROTON/ELECTRON RATIOS

Expanding on Schlickeiser (2002), let us assume that electrons and protons are accelerated out of a thermal bath, characterized by a non-relativistic kinetic energy $T_0 \simeq 10\,\mathrm{keV}$, to a differential PL spectrum (in momentum) $N_{\rm j}(p) = N_{0,{\rm j}} p^{-q_{\rm j}}$ where j=e,p. At injection, $q_{\rm e} = q_{\rm p}$. Later, different loss and diffusion processes for the two CR species will in general result in $q_{\rm e} \neq q_{\rm p}$. If electrical neutrality of primary CRs is conserved, then the total number of CR particle of each species per volume unit is

$$n_o \;=\; \int_{T_0}^{\infty} N_{\rm e}(T)\,{\rm d}T \;=\; \int_{T_0}^{\infty} N_{\rm p}(T)\,{\rm d}T\,. \tag{15}$$

The energy-momentum relation $T{=}\sqrt{m^2c^4+p^2c^2}{-}mc^2$ implies $p{=}\sqrt{T^2/c^2+2Tm}$ and ${\rm d}p/{\rm d}T{=}(T/c^2+m)(T^2/c^2+2Tm)^{-1/2}$. As $N_{\rm j}(T){=}N_{\rm j}[p(T)]{\rm d}p/{\rm d}T$, the final expression is (see Schlickeiser 2002)

$$N_{\rm j}(T) \;=\; \frac{N_{0,{\rm j}}}{c^2}\,(T+mc^2)\,\Big(\frac{T^2}{c^2}+2Tm\Big)^{-(q_{\rm j}+1)/2}. \tag{16}$$

Inserting Eq.(16) in Eq.(15), we obtain the normalization of each CR species,

$$N_{0,{\rm j}} \;=\; (q_{\rm j}-1)\;n_0\,\Big(\frac{T_0^2}{c^2}+2T_0m\Big)^{(q_{\rm j}-1)/2}. \tag{17}$$

Because of the assumed electrical neutrality of the primary CRs, we get

$$\frac{N_{0,{\rm p}}}{N_{0,{\rm e}}} \;=\; \frac{q_{\rm p}-1}{q_{\rm e}-1}\;\frac{\big[m_{\rm p}+(T_0/2c^2)\big]^{(q_{\rm p}-1)/2}}{\big[m_{\rm e}+(T_0/2c^2)\big]^{(q_{\rm e}-1)/2}}\;\frac{(2T_0)^{(q_{\rm p}-1)/2}}{(2T_0)^{(q_{\rm e}-1)/2}} \;\simeq$$

$$\simeq\; \frac{q_{\rm p}-1}{q_{\rm e}-1}\;\frac{(2T_0m_{\rm p})^{(q_{\rm p}-1)/2}}{(2T_0m_{\rm e})^{(q_{\rm e}-1)/2}} \tag{18}$$

since $T_0 << m_{\rm e}c^2 << m_{\rm p}c^2$.

- The p/e number density ratio is

$$\omega(T;q_{\rm p},q_{\rm e}) \;=\; \frac{N_{\rm p}(T)\,{\rm d}T}{N_{\rm e}(T)\,{\rm d}T}\,. \tag{19}$$

Inserting Eqs.(16),(18) in Eq.(19), we obtain

$$\omega(T;q_{\rm p},q_{\rm e}) \;=\; \frac{(q_{\rm p}-1)}{(q_{\rm e}-1)}\;\frac{\big(2T_0m_{\rm p}c^2\big)^{\frac{q_{\rm p}-1}{2}}}{\big(2T_0m_{\rm e}c^2\big)^{\frac{q_{\rm e}-1}{2}}}\;\times$$

$$\times\;\frac{T^{1-q_{\rm p}}(T+m_{\rm p}c^2)(T+2m_{\rm p}c^2)^{-\frac{q_{\rm p}+1}{2}}}{T^{1-q_{\rm e}}(T+m_{\rm e}c^2)(T+2m_{\rm e}c^2)^{-\frac{q_{\rm e}+1}{2}}}\,. \tag{20}$$

From Eq.(20) it is straighforward to see that at injection, when $q_{\rm p} = q_{\rm e} = q_{\rm inj}$, it is (Schlickeiser 2002)

$$\omega(T;q_{\rm inj}) \begin{cases} = 1... & ...\; T/c^2 << m_{\rm e} \\ \propto \Big(\frac{T}{m_{\rm p}c^2}\Big)^{\frac{q_{\rm inj}-1}{2}} & ...\; m_{\rm e} << T/c^2 << m_{\rm p} \\ = \Big(\frac{m_{\rm p}}{m_{\rm e}}\Big)^{\frac{q_{\rm inj}-1}{2}} & ...\; T >> m_{\rm p}c^2\;. \end{cases} \tag{21}$$

Notice that for $q_{\rm inj} \simeq 2.2$, $\omega(T >> 1\,{\rm GeV}) \simeq 10^2$, as remarked by Schlickeiser (2002).

- The p/e energy density ratio is

$$\kappa(q_{\rm p},q_{\rm e}) \;=\; \frac{\int_{T_0}^{\infty} N_{\rm p}(T)\,T\,{\rm d}T}{\int_{T_0}^{\infty} N_{\rm e}(T)\,T\,{\rm d}T}\,. \tag{22}$$

Inserting Eqs.(16),(18) in Eq.(22), we obtain

$$\kappa(q_{\rm p}, q_{\rm e}) \; = \; \frac{(q_{\rm p}-1)}{(q_{\rm e}-1)} \, \frac{(2T_0 m_{\rm p} c^2)^{\frac{q_{\rm p}-1}{2}}}{(2T_0 m_{\rm e} c^2)^{\frac{q_{\rm e}-1}{2}}} \times$$

$$\times \, \frac{\int_{T_0}^{\infty} T^{-\frac{q_{\rm p}-1}{2}} (T+m_{\rm p}c^2)(T+2m_{\rm p}c^2)^{-\frac{q_{\rm p}+1}{2}} {\rm d}T}{\int_{T_0}^{\infty} T^{-\frac{q_{\rm e}-1}{2}} (T+m_{\rm e}c^2)(T+2m_{\rm e}c^2)^{-\frac{q_{\rm e}+1}{2}} {\rm d}T} \, . \qquad (23)$$

Calling the integrand functions on the top and bottom of the r.h.s. of Eq.(22), respectively, $f_{\rm p}(T)$ and $f_{\rm e}(T)$, we can rewrite $\int_{T_0}^{\infty} f_{\rm p}(T){\rm d}T = \int_{T_0}^{m_{\rm p}c^2} f_{\rm p}(T){\rm d}T + \int_{m_{\rm p}c^2}^{\infty} f_p(T){\rm d}T$ and $\int_{T_0}^{\infty} f_{\rm e}(T){\rm d}T = \int_{T_0}^{m_{\rm e}c^2} f_{\rm e}(T){\rm d}T + \int_{m_{\rm e}c^2}^{\infty} f_{\rm e}(T){\rm d}T$. Hence, in the approximations $T << m_{\rm p}c^2, T >> m_{\rm p}c^2$ and, respectively, $T << m_{\rm e}c^2, T >> m_{\rm e}c^2$, we can write Eq.(23) as

$$\kappa(q_{\rm p}, q_{\rm e}) \; \simeq \; \frac{(q_{\rm p}-1)}{(q_{\rm e}-1)} \, \frac{(2T_0 m_{\rm p} c^2)^{\frac{q_{\rm p}-1}{2}}}{(2T_0 m_{\rm e} c^2)^{\frac{q_{\rm e}-1}{2}}} \times$$

$$\times \, \frac{(2m_{\rm p}c^2)^{-\frac{q_{\rm p}-1}{2}} \frac{1}{3-q_{\rm p}} T^{3-q_{\rm p}} \Big|_{T_0}^{m_{\rm p}c^2} + \frac{1}{2-q_{\rm p}} T^{2-q_{\rm p}} \Big|_{m_{\rm p}c^2}^{\infty}}{(2m_{\rm e}c^2)^{-\frac{q_{\rm e}-1}{2}} \frac{1}{3-q_{\rm e}} T^{3-q_{\rm e}} \Big|_{T_0}^{m_{\rm e}c^2} + \frac{1}{2-q_{\rm e}} T^{2-q_{\rm e}} \Big|_{m_{\rm e}c^2}^{\infty}} \, , \qquad (24)$$

where $T_0 = 10^{-5}\,$GeV, $m_{\rm e}c^2 = 0.511 \times 10^{-3}\,$GeV, $m_{\rm p}c^2 = 0.94\,$GeV. Note that at injection $q_{\rm p} = q_{\rm e} = q_{\rm inj}$, so that

$$\kappa(q_{\rm inj}) \; \simeq \; \Big(\frac{m_{\rm p}}{m_{\rm e}}\Big)^{\frac{3-q_{\rm inj}}{2}} \quad \ldots \;\; T >> 1\,{\rm GeV}\, . \qquad (25)$$

Eq.(25) is the counterpart of the third of Eqs.(21).

Eq.(24) enforces electric neutrality of the primary CRs for any pair of $q_{\rm p}$, $q_{\rm e}$. In computing κ from Eq.(24) we assume $q_{\rm e}$ to be measured from radio data according to standard synchrotron theory, $q_{\rm e} = 2\alpha + 1$. However, the CRp spectral index, $q_{\rm p}$, is not directly measurable hence some guess must be made:

(a) in starburst regions, that are sources of primary CRs, we assume the average CRp spectral index to stay close to the injection index, $q_{\rm p} \sim q_{\rm inj}$: as VHE γ-ray observations of SN remnants suggest $q_{\rm inj} \simeq 2.2$ (Aharonian et al. 2006), we assume $q_{\rm p} \simeq 2.2$ in starburst cores;

(b) in quiescent galaxies like the Milky Way, small source regions are mixed with large passive regions, so that in the regions typically sampled in these galaxies, CRp are mostly affected by confinement effects only (leaky-box model: homogeneous distribution of CRp sources, no CRp energy losses, CRp confinement time scaling inversely with energy), and the steady-state solution of the diffusion-loss equation yields $q_{\rm p} = q_{\rm inj} + \delta$ [2]. Because $\delta \simeq 0.5$ (Gupta & Webber 1989), we assume a spectral index $q_{\rm p} = 2.7$ for CRp in quiescent galaxies.

---

[2] The general diffusion-loss equation is $\frac{\partial N(E)}{\partial t} = D\nabla^2 N(E) - \frac{N(E)}{\tau(E)} + \frac{\rm d}{{\rm d}E}[b(E)N(E)] + Q(E)$ (Ginzburg & Syrovatskii 1964) where D is the scalar diffusion coefficient, $Q(E)$ is the source term, $\tau(E)$ is the energy-dependent time confinement timescale, $b(E)$ is the energy loss rate, $N(E)$ is the steady-state distribution of particles. At steady state ($\frac{\partial N(E)}{\partial t=0}$), for a homogeneous distribution of sources ($D\nabla^2 N(E) = 0$) and negligible CR energy losses ($b(E) = 0$), the loss-diffusion equation becomes $N(E) = Q(E)\tau(E)$ (leaky-box model). Since $\tau(E) \propto E^{-\delta}$, assuming $Q(E) \propto E^{-q_{\rm inj}}$ we get $N(E) \propto E^{-(q_{\rm inj}+\delta)}$.